Available online at www.sciencedirect.com
ScienceDirect
Acta Materialia 70 (2014) 240–248
Acta MATERIALIA
www.elsevier.com/locate/actamat

Icosahedral quasicrystal-enhanced nucleation of the fcc phase in liquid gold alloys

Güven Kurtuldu [a,*], Alberto Sicco [a,b], Michel Rappaz [a]

[a] Computational Materials Laboratory, Institute of Materials, Ecole Polytechnique Fédérale de Lausanne, Station 12, CH-1015 Lausanne, Switzerland
[b] Rolex SA, 3-5-7 Rue François-Dussaud, 1211 Geneva 26, Switzerland

Received 22 January 2014; accepted 25 February 2014

Abstract

Although the grain refinement of yellow gold alloys with Ir has been used in industry and known for nearly half a century, the basic mechanism is still unknown. The present contribution shows that the mechanism is the same as that evidenced recently in Al–Zn alloys, when small amounts of Cr (1000 ppm) are added to the melt (Kurtuldu et al., 2013). The reduced face-centered cubic (fcc) crystal size, the abnormal fraction of twin, or near-twin, grain boundaries and the 5-fold symmetry crystallographic orientation of multiple nearest-neighbor grains reproduce the symmetry of icosahedral quasicrystals (iQCs) with the following heteroepitaxial relationships: $\{1\,1\,1\}_{fcc}/\langle 1\,1\,0\rangle_{fcc}\perp$ 3-fold/2-fold symmetry axes of iQCs. While iQCs and the approximant stable $Al_{45}Cr_7$ phase, which contains several 5-fold symmetry building blocks in its unit cell, are known to exist in Al–Cr alloys, no such phases have been reported for yellow gold +Ir. Nevertheless, when minute amounts of Ir ($\lesssim$ 200 ppm) are added to the gold alloy melt, it is shown that the grain refinement from 248 to 30 μm is accompanied by a spectacular increase in the fraction of twinned grain boundaries, i.e. from less than 1% without Ir to 11% with 200 ppm Ir. Furthermore, up to 9 grains have been shown to reproduce the six 5-fold symmetry axes of the icosahedron, while many other grain configurations exhibit this heteroepitaxial relationship with the icosahedron or interlocked icosahedron. This confirms that fcc crystals can form in a supercooled liquid by heteroepitaxial growth from an iQC template.

Keywords: Nucleation; Icosahedral quasicrystals; Multiple twinning; Heteroepitaxy; Grain refinement

1. Introduction

In order to explain the large supercoolings of metallic liquids observed by Turnbull [1], Frank [2] suggested in 1952 that atoms in metallic liquids develop short-range icosahedral order when the temperature is reduced below the equilibrium freezing point. Molecular dynamics simulations [3,4] and small-angle scattering in various metallic liquids [5–8] confirmed this conjecture. More recently, Shechtman et al. [9] discovered quasicrystals (QCs) in a rapidly solidified Al–Mn alloy, thus changing our view on crystallography. While exhibiting long-range order and 5-fold symmetry, QCs do not possess translational order. Although metastable Al–Mn QCs were shown to remain stable for 1 h up to 350 °C, they transformed into the approximant Al_6Mn phase above this temperature. After this discovery, for which Shechtman won the Nobel prize in 2011, thermodynamically stable QCs were found in binary [10,11] and ternary alloys [12–14], and were grown into grains several millimeters in size.

Interestingly, Shechtman et al. [9] had already noticed that crystalline films of face-centered cubic (fcc) Al formed around nodular shaped QCs, which is expected for such a peritectic system, but did not investigate further if there

* Corresponding author.
E-mail addresses: guven644@yahoo.com, guven.kurtuldu@epfl.ch (G. Kurtuldu).

http://dx.doi.org/10.1016/j.actamat.2014.02.037
1359-6454/

were some cystallographic relationships between these films and QCs. Singh and Tsai [15] demonstrated that epitaxial crystallographic relationships exist between the α-Mg phase and Mg–Zn–Y QCs, as well as between Pb, Bi and Sn particles embedded in an icosahedral Al–Cu–Fe matrix. Crystallographic relationships were also found between QCs and approximant intermetallic phases [16–18], in particular in rapidly solidified Al–Cr alloys. In vapor-deposited Al films on Al–Pd–Mn icosahedral QC (iQC), an epitaxial relationship between the fcc phase and QCs was observed, with the $\langle 1\,1\,1\rangle_{fcc}$ direction parallel to one of the 3-fold symmetry axes of the icosahedron [19,20].

We have recently shown that iQCs can also play a role in the nucleation of the fcc Al phase during solidification of an Al–20 wt.%Zn alloy [21]. Small additions of Cr (1000 ppm) in the liquid metal drastically decrease the size of the fcc grains and induce an abnormally high fraction of twin or near-twin grain boundaries ($> 2\%$). By careful analysis of the orientation of nearest-neighbor fcc grains, we also found several configurations where multiple-twinned grains exhibited a symmetry which could be explained only if they were assumed to form on a single regular or interlocked icosahedron with the epitaxial relationship: $\langle 1\,1\,1\rangle_{fcc} \| 3$-fold symmetry iQC axes, and $\langle 1\,1\,0\rangle_{fcc} \perp 2$-fold symmetry iQC axes. This provided compelling evidence supporting the concept that fcc grains could nucleate from an icosahedral template, known to be present as iQCs in the supercooled liquid or as building blocks of the crystalline structure of the approximant $Al_{45}Cr_7$ phase [22,23]. The phase initiated from a melt can be the one that is closest in free energy to the liquid, not the thermodynamically most stable one [24]. Metastable iQC in supercooled metallic liquid is the most likely candidate to form initially due to its low interfacial energy [25,26]. Indeed, Kelton et al. [27] have demonstrated that the icosahedral short-range order first grows into a metastable iQC phase, then transforms into a more stable crystalline phase in a supercooled $Ti_{39.5}Zr_{39.5}Ni_{21}$ liquid.

This iQC-induced nucleation is schematically summarized in Fig. 1. In Fig. 1a, Al and Zn atoms (in blue) tend to arrange around Cr atoms (in red) in Frank's configuration. The liquidus temperature of the approximant $Al_{45}Cr_7$ being above that of the fcc phase in this alloy, iQCs (or the approximant phase itself) form at some undercooling (Fig. 1b). As the Al–Cr system is peritectic, the liquid layer ahead of the iQC is depleted in Cr, thus favoring the formation of the fcc (Al–Zn) phase, with epitaxial relationships (Fig. 1c). Upon further solidification and cooling, the iQC disappears while the fcc phase grows with multiple twin or near-twin relationships between the various grains, as indicated in Fig. 1d. Once the fcc phase reaches a critical radius, the solid–liquid interface is destabilized, thus leading to the formation of twinned dendrites [28,29,21], a morphology known in industrial direct chill-cast Al alloys for more than 60 years and whose origin could not be explained before this nucleation mechanism was demonstrated.

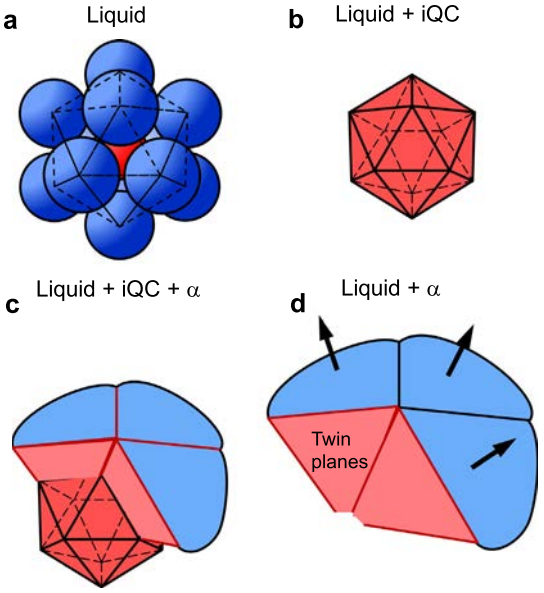

Fig. 1. Nucleation mechanism assisted by iQC formation: (a) Frank's icosahedral short-range order of atoms in the liquid (red: Cr atoms; blue: Al or Zn atoms); (b) formation of iQC in the liquid; (c) heteroepitaxy of the α-fcc phase on the iQC facets, with twin planes in between the various α nuclei; (d) growth of the fcc phase and dissolution of the iQC during cooling due to the peritectic nature of the phase diagram. (For interpretation of the references to color in this figure legend, the reader is referred to the web version of this article.)

In this paper, the same nucleation mechanism is shown to operate in yellow gold alloys (Au–12.5 wt.%Cu–12.5 wt.%Ag or Au–28.4 at.%Cu–16.7 at.%Ag) when minute amounts of Ir (5–200 wt. ppm) are added to the melt. "Inoculation" of such alloys with Ir is a grain-refining technique currently used in industry and known for nearly half a century [30–32]. However, although the effect of Ir on grain size is well established, there has been no investigation on the basic mechanism responsible of such grain refinement.

2. Experimental methods

Ingots of 700 g of Au–28.4 at.%Cu–16.7 at.%Ag alloys (purity Au, Ag, Cu: 99.99%) with a suitable amount of Ir (in the form of Cu–0.67 at.%Ir) were prepared in a vacuum induction furnace under an argon atmosphere. The mixed elements were heated in a graphite crucible. The temperature was brought up to 1300 °C for 5 min and then reduced to 1100 °C, where it stabilized for another 5 min. The ingots were cast at 1100 °C into copper molds ($20 \times 20 \times 100$ mm^3) at room temperature. Samples were cut at about two-thirds from the top of the ingot and prepared for electron backscattered diffraction (EBSD) analysis by polishing with 0.5 μm alumina suspension (OPS) and by subsequent etching with KCN. Optical and electron microscopy as well as EBSD observations were made on yellow gold specimens containing 5, 10, 20, 30, 50, 100 and 200 wt. ppm Ir. A Phillips XLF-30 FEG SEM with

an HKL detector was used for that purpose and analysis of the reconstructed EBSD maps to identify twin boundaries was made with a tolerance of 5°.

3. Results and discussion

Fig. 2 shows false-color EBSD maps of as-solidified Au–Cu–Ag alloys without and with 20 and 200 ppm Ir additions. The three color components of the grains correspond to their three Euler angles, and identified twin grain boundaries are outlined with white lines. Ir has a drastic effect on the grain size, as expected from the known literature: the grain size is about 250 μm in the specimen without Ir addition, and only 30 μm in the specimen with 200 ppm Ir (i.e. the grain density is multiplied by 600). This grain refinement is accompanied by a spectacular increase in the fraction of twinned grain boundaries, from less than 1% without Ir to 11% with 200 ppm Ir. The grain boundary

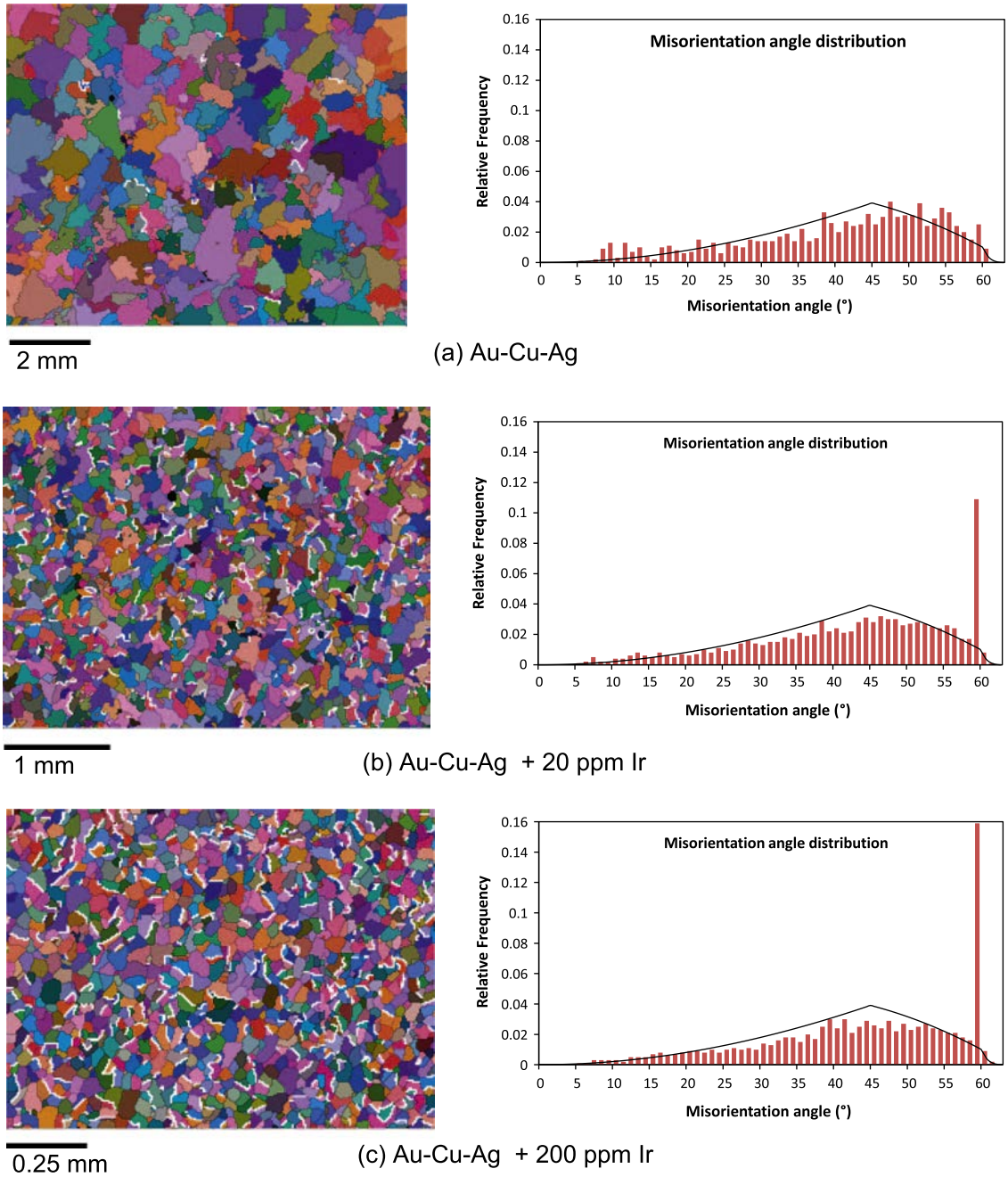

Fig. 2. EBSD reconstructed maps of as-cast Au–Cu–Ag alloys (a) without and with (b) 20 ppm or (c) 200 ppm Ir additions to the melt. The color of the grains corresponds to their three measured Euler angles and twin grain boundaries are indicated by white lines. For each EBSD map, misorientation angle distributions between neighboring grains are also shown. The grain boundary misorientation histograms of the samples are compared with the theoretical distribution of randomly nucleated grains (continuous black curves, Mackenzie plot [33]). The peak appearing at 60° corresponds mostly to twins, since a twin can also be viewed as a rotation of 60° of the crystallographic lattice around a common ⟨1 1 1⟩ direction. (For interpretation of the references to color in this figure legend, the reader is referred to the web version of this article.)

misorientation distributions of these alloys can also be seen in Fig. 2. While a few twinned grain boundaries are present in yellow gold alloys without Ir addition, many twinned grains are formed when Ir is added as shown by EBSD reconstructed maps. From the orientation of the grains, a statistics of the grain misorientation can be made. The relative orientation of one grain with respect to its neighbor can be described by three Euler angles, or alternatively by one rotation axis (two variables) and a rotation angle. Fig. 2 shows the statistics of this rotation angle between two adjacent grains. These experimental histograms can be compared with the misorientation distribution of randomly oriented grains of cubic symmetry, known as a Mackenzie plot (black continuous curves) [33]. For regular gold alloys without Ir in Fig. 2a, the experimental histogram follows fairly well the random distribution. When an increasing amount of Ir is added (Fig. 2b and c), a peak of increasing intensity appears at 60°. This corresponds to twin boundaries, since a twin corresponds to a rotation of 60° of the lattice around a common ⟨1 1 1⟩ direction. These EBSD measurements show the correlation between the grain refinement effect of Ir on yellow gold alloys and the increasing percentage of twin boundaries.

To further investigate the effect of Ir addition, various EBSD measurements were performed on as-cast gold alloys containing 5, 10, 30, 50 and 100 wt. ppm Ir. Fig. 3 shows the effect of different amounts of Ir addition on the grain size and frequency of twins. The error bars for the grain size correspond to the standard deviation of the distribution. With only 5 ppm addition of Ir, the grain size drops from 250 to 90 μm. Further addition of Ir continues to reduce the grain size, but to a lower extent. The grain size drops to about 60–70 μm for 10–50 ppm Ir addition and further decreases to 30–40 μm with 100–200 ppm Ir addition. Two phenomena can explain this saturation effect. (i) The final grain structure in a solidified alloy is a convolution of nucleation and growth. Once the first grains form, they grow and can entrap other potential nucleation sites. In order to further refine the grain size, growth should then be impeded by increasing the cooling rate. (ii) For the highest Ir compositions, we have observed by scanning electron microscopy the precipitation of a few Ir particles (typically 1–2 μm in size), indicating that they had formed in the liquid, i.e. the Ir solubility limit of the alloy has been exceeded.

The frequency of twin boundaries, i.e. the ratio of boundaries between two grains exhibiting a twin relationship within a tolerance of 5° over the total number of grain boundaries, is shown on the second vertical axis in Fig. 3. The error bars for twin density correspond to a 99% confidence interval for the corresponding total number of grain boundaries. For a random orientation of a grain with respect to a reference grain, the probability of having a twin relationship within a 5° tolerance between them is 0.3% [34]. For gold alloy without Ir, the frequency of twin formation is $0.82\% \pm 0.53\%$. This greater-than-random value could be attributed to the same mechanism induced by uncontrolled impurity elements, or to the formation of a few spontaneous stacking faults at the fcc Au–liquid interface (which then lead to twins upon growth) since gold is known to have a low stacking fault energy [35]. When Ir is added to gold alloys, as can be seen in Fig. 3, the density of twins increases significantly, reaching 10.9% for alloy containing 200 ppm Ir. This value is different from the relative frequency of grain boundary misorientation distribution at 60° (Fig. 2), because grains having 60° misorientation do not always have a twin relationship and also because the relative frequency in Fig. 2 gives information on the length of the grain boundaries with a certain misorientation relative to the total length of the grain boundaries.

The relationship between the grain size and fraction of twin grain boundaries is summarized in Fig. 4 for all the Ir compositions. While the grain size values are grouped as 248, 90, 60–70 and 30–40 μm for 0, 5, 10–50 and 100–200 ppm Ir contents, respectively, the frequency of occurrence of twins can be grouped as 0.82, 2.84, 7.4–8.1 and 10.7–10.9% for 0, 5, 10–50 and 100–200 ppm Ir contents, respectively. This shows that addition of Ir continues to decrease the grain size, if and only if it promotes the formation of twin boundaries. As for Al alloys in which a few ppm of Cr are added, this already gives a very significant clue as to the nucleation mechanism of the fcc phase in gold alloys inoculated with a few ppm of Ir. However, in order to prove that this nucleation mechanism is similar to that

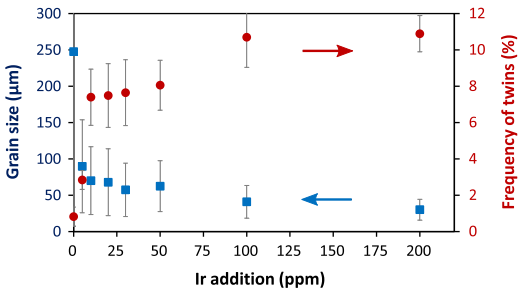

Fig. 3. Grain size and frequency of twins as a function of Ir addition in Au–Cu–Ag alloys. While error bars show the standard deviation for grain size, they show the error limits for twin frequency with a confidence interval of 99%.

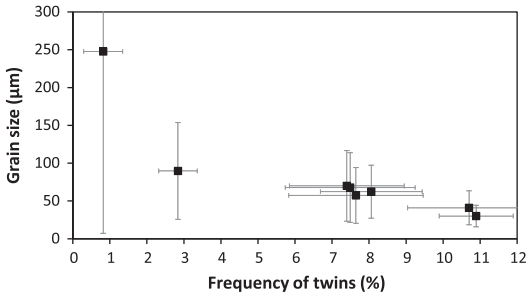

Fig. 4. Grain size vs. frequency of twins in Au–Cu–Ag alloys with or without Ir addition. Error bars show the standard deviation for grain size and the error limits for frequency of twins with a confidence interval of 99%.

identified in Al–Zn–Cr alloys (see Fig. 1), multiple-twin orientation relationships between several fcc grains must be identified.

Further detailed EBSD investigations of Ir-inoculated gold alloys revealed several grains having multiple twin relationships between three, four and five grains having a common ⟨1 1 0⟩ direction as shown in Fig. 5.

Fig. 6a shows the EBSD reconstructed map of an occurrence of nine grains in a 20 ppm Ir–gold alloy exhibiting multiple twin or near-twin relationships between them. For a better visibility and understanding, their crystallographic orientation are grouped into six ⟨1 1 0⟩ pole figures (Fig. 6c–h) according to grains sharing a nearly common ⟨1 1 0⟩ direction. In the pole figures, each grain orientation is shown with the same color as in Fig. 6a and "useless" ⟨1 1 0⟩ directions (i.e. not contributing to the understanding of multiple twin relationships) are discarded. Common or nearly common {1 1 1} planes of the various fcc grains are represented as arcs of circle, and common or nearly common directions of more than two grains are encircled. Finally, in order to relate these orientations with a common icosahedron template, an icosahedron with 10 visible facets has been drawn in Fig. 6b with an orientation approximately corresponding to that deduced from the pole figures. The triangular facets of the icosahedron are numbered and colored in a way corresponding to the fcc grains in Fig. 6a. The six 5-fold symmetry axes of the icosahedron have been labeled (c)–(h) and their position in the pole figure (Fig. 6b) corresponds to that of the ⟨1 1 0⟩ common direction of the grains in the pole figures (Fig. 6c–h).

In Fig. 6c, the ⟨1 1 0⟩ pole figure of grains 1–5 shows a twin relationship between the set of grains 1/2, 2/3, 3/4 and 4/5, and a near-twin relationship between grains 5/1, all sharing a common ⟨1 1 0⟩ direction (circled in this figure and labeled (c) in the icosahedron of Fig. 6b). This near-twin relationship, defined in Ref. [21], corresponds to a rotation of 7° of the nearly common {1 1 1} plane along a common ⟨1 1 0⟩ direction in order to match the opening deficiency of five side-by-side {1 1 1} tetrahedra. Indeed, regular tetrahedra in an fcc crystal have four {1 1 1} triangular facets and six ⟨1 1 0⟩ edges. Two side-by-side fcc tetrahedra sharing a common {1 1 1} twin plane and three ⟨1 1 0⟩ edges are in a perfect twin relationship. When five such tetrahedra share a common ⟨1 1 0⟩ direction, they form almost a pentagonal dipyramid, but with a gap of 7.35° between the closest {1 1 1} planes of the first and last tetrahedra. Assuming these five fcc gold grains form on a perfect icosahedral (or dipyramidal) nucleation template,

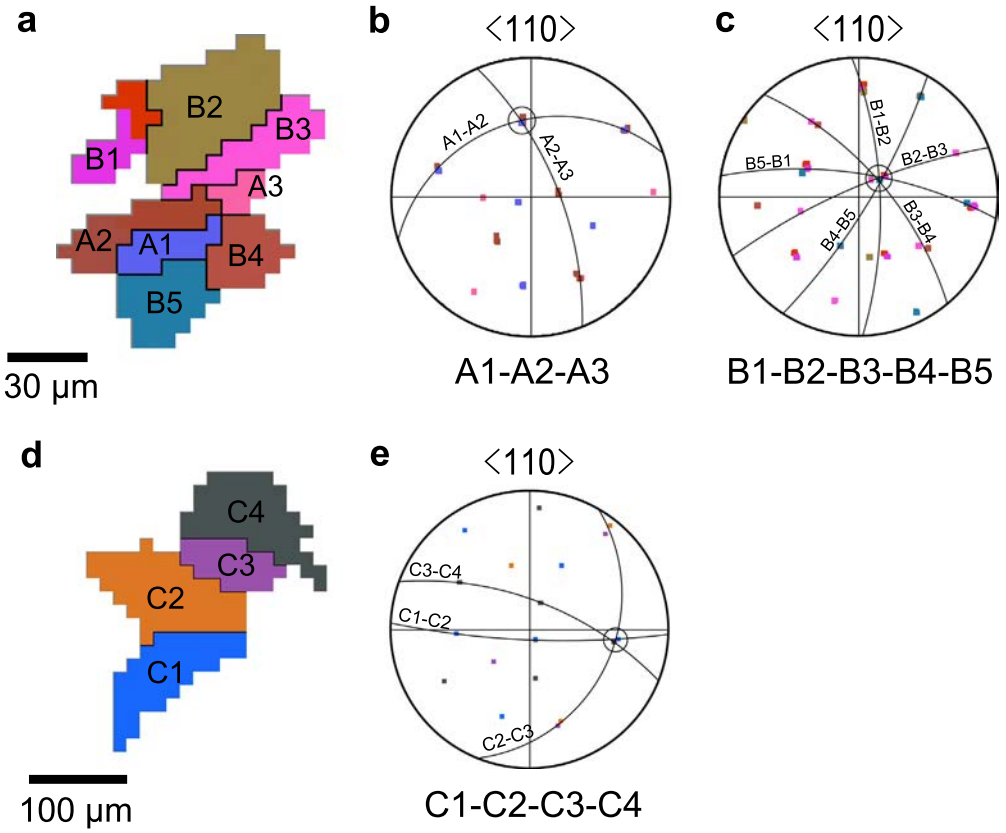

Fig. 5. (a) EBSD reconstructed map of grains in Au–Cu–Ag alloy with 200 ppm Ir having multiple twin relationship with each other. The ⟨1 1 0⟩ pole figures show the multiple twin relationships with a common or near-common ⟨1 1 0⟩ direction (b) between grains A1/A2/A3 and (c) between grains B1/B2/B3/B4/B5. (d) EBSD map of grains in Au–Cu–Ag alloy with 20 ppm Ir having four multiple twinned grains C1/C2/C3/C4 as shown in (e) by the corresponding ⟨1 1 0⟩ pole figure. The common or nearly common {1 1 1} planes are displayed in each pole figure by arcs of circle and common ⟨1 1 0⟩ directions of a multiple twin relationship are shown by a single circle in each pole figure.

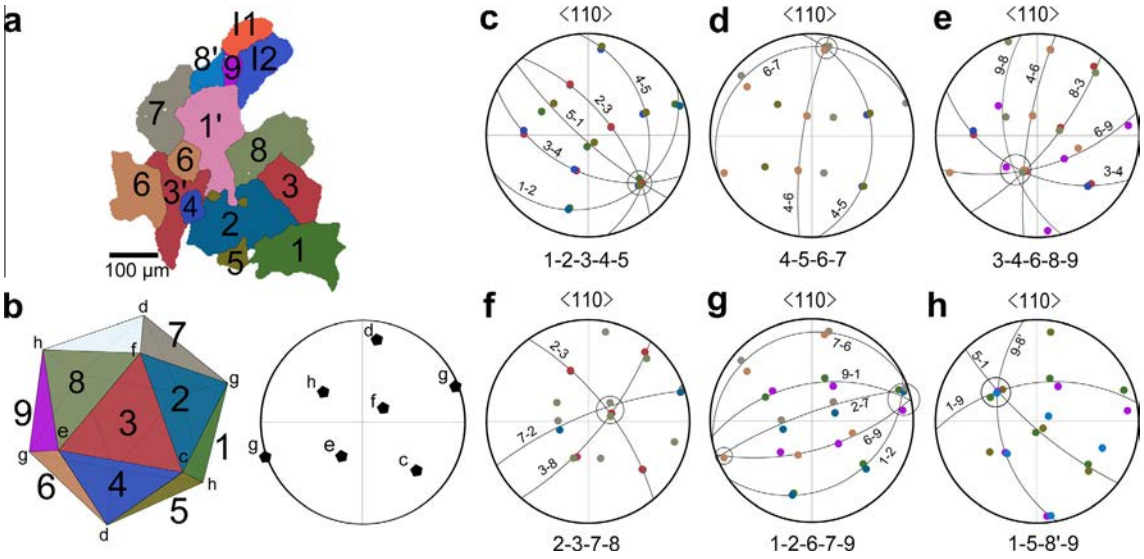

Fig. 6. Crystallographic relationships of nine grains in Au–Cu–Ag alloy with 20 ppm Ir. (a) EBSD reconstructed map of the grains. The corresponding ⟨1 1 0⟩ pole figures of these grains shown in (c)–(h) are grouped in such a way as to reveal the six common 5-fold symmetry axes of an icosahedron labeled with the same letter in (b). A perfect icosahedron positioned with about the same orientation is also shown in (b) with facets from which the fcc phase formed having the same color and number as the grains in (a). The common or nearly common {1 1 1} planes are displayed in each pole figure by arcs of circle, while the 5-fold nearly common ⟨1 1 0⟩ directions of four or five grains in (c)–(h) are circled. Note that unnecessary ⟨1 1 0⟩ directions, i.e. those that are not common to at least two grains, are not represented in the pole figures for the sake of clarity. Grains with a primed number have the same or nearly same orientations as the corresponding unprimed grain (e.g. 8 and 8′). (For interpretation of the references to color in this figure legend, the reader is referred to the web version of this article.)

this 7.35° deficiency should be shared equally between them (i.e. the five nearly common {1 1 1} planes of these five grains should exhibit a misorientation of 1.47° along the common ⟨1 1 0⟩ direction between two neighbors). However, besides the precision of EBSD measurements which is of the order of 2°, subgrain misorientations develop during grain growth, and since coherent twin boundaries exhibit a sharp cusp in the grain boundary energy [36], it is not surprising that this opening deficiency is "concentrated" on a single near-twin boundary.

Already at this stage, it is fairly evident that the five fcc gold grains labeled 1–5 in Fig. 6 must have formed on a template having the 5-fold symmetry of a pentagonal dipyramid. The other orientation relationships shown by grains 1–9 in the pole figures Fig. 6d–h indicate that the template is in fact an icosahedron, i.e. with five supplementary 5-fold symmetry axes labeled (d)–(h) in Fig. 6b. However, when comparing the orientation relationships of these nine fcc grains with the symmetry properties of the icosahedron, it should be kept in mind that the deficiency gap of 7.35° built in the pentagonal dipyramid cumulates when the other 5-fold symmetry axes are added for the construction of the icosahedron from 20 {1 1 1} tetrahedra.

The ⟨1 1 0⟩ directions of grains 4, 5, 6 and 7 are shown in the pole figure of Fig. 6d. These four grains share three common or nearly common {1 1 1} planes having a common ⟨1 1 0⟩ direction (circled in this figure and identified as (d) in Fig. 6b). The fifth grain sharing this common ⟨1 1 0⟩ direction could not be found in the metallographic cross-section. Note that grains 6 and 7 have a near-twin relationship, while the two other sets of grains (4/5 and 4/6) are in a perfect twin relationships.

The third 5-fold axis of the icosahedron, labeled (e) in Fig. 6b, appears via the orientation relationships of the five grains 3, 4, 6, 8 and 9 shown in Fig. 6e. The pairs of grains 3/4, 3/8 and4/6 are in perfect twin relationships, but the misorientations between 6/9 and 8/9 are larger. Grains 6 and 9 share a common {1 1 1} plane (arc of circle) but the three ⟨1 1 0⟩ directions in this plane are slightly rotated along a common ⟨1 1 1⟩ direction. This rotation of grain 9 with respect to grain 6 is also reflected in the orientation relationship with its other neighbor, grain 8. While grains 3, 4, 6 and 8 are rotated around a common ⟨1 1 0⟩ direction, that of grain 9 is misoriented by about 10°. While another name could be found for this pseudo-twin relationship between grain 9 and its neighbors, the misorientation still comes from the gap deficiency of the pile-up of $\{1\,1\,1\}_{fcc}$ tetrahedra, which cumulates when 20 of them form on a regular icosahedron.

Only four grains have been found in the metallographic cross-section to identify the fourth 5-fold symmetry axis (f) of the icosahedron (Fig. 6f, grains 2, 3, 7 and 8). The two sets of grains 2/3 and 3/8 have a twin relationship, while grains 2/7 are in a pseudo-twin relationship identical to that of grains 1/5. The missing grain (uncolored facet on the icosahedron in Fig. 6b), is on the opposite facet of the icosahedron where another grain of the 5-fold symmetry was already absent (missing grain in the set 4, 5, 6 and 7 of the symmetry shown in Fig. 6d). It is worth noting that two opposite facets of an icosahedron are parallel, with edges of the triangle also parallel but turned 180° with

respect to each other. Thus, fcc crystals forming on two opposite facets of the icosahedron have the same orientation (if one neglects the gap deficiencies). This is why grain 7, which clearly belongs to the set of grains sharing the 5-fold symmetry axis (f) (grains 2, 3, 7 and 8), also appears in the set of grains 4, 5, 6 and 7 (5-fold symmetry axis (d)) while it does not appear to share any common edge on the icosahedron of (b). When such occurrence happens, i.e. a grain appearing in the cross-section and sharing a symmetry property with others but coming from the opposite facet of the icosahedron, the prime symbol is used (e.g. 1′, 3′, 8′).

The misorientation of grain 9 with respect to its neighbors 6 and 8 in Fig. 6e also appears in the pole figure (Fig. 6g) with its third neighbor 1 or 1′ which has a similar crystal orientation as grain 1 (rotation of 11° around a common ⟨1 1 0⟩). Except for this misorientation, the orientations of the grains 1, 2, 6, 7 and 9 shown in the pole figure (Fig. 6g) share a nearly common ⟨110⟩ direction which corresponds to the fifth 5-fold symmetry axis of the icosahedron (see Fig. 6b). Finally, the last 5-fold symmetry axis of the icosahedron appears in the orientation of the fcc grains 1, 5, 8′ and 9 (Fig. 6h). The crystal orientation of grain 8′ is very close to that of grain 8 (rotation of 15° around a common ⟨1 0 0⟩ direction).

Fig. 7 shows that, different from twin or near-twin relationships, there is another relation between the gold grains 8′, 9, I1 and I2, which was also observed in Al–Zn–Cr alloys [21]. Their ⟨1 1 0⟩, ⟨1 1 1⟩ and ⟨2 1 1⟩ pole figures are given in Fig. 7c–e. As can be seen from these pole figures, the grain sets 8′/9 and I1/I2 are in a twin relationship. The common ⟨1 1 0⟩ and ⟨1 1 1⟩ directions of these two pairs are circled in the ⟨1 1 0⟩ and ⟨1 1 1⟩ pole figures. However, twinning is not the only relationship existing between these four grains. These two pairs share a common ⟨2 1 1⟩ direction, double circled in the ⟨2 1 1⟩ pole figure, and their crystallographic configurations are simply rotated by 63° around this direction. Furthermore, grains 8′ and I2 share a common ⟨1 1 0⟩ direction (circled in green), while grains 9 and I1 share another common ⟨1 1 0⟩ direction (circled in red). The crystallographic relationships between these four grains can be understood if one considers the four triangular facets labeled 8′, 9, I1 and I2 of the interlocked icosahedron shown in Fig. 7b. Assuming again epitaxial growth of the α-phase on the facets of this interlocked icosahedron, it can be seen that: (i) tetrahedra 8′ and 9, as well as I1 and I2,

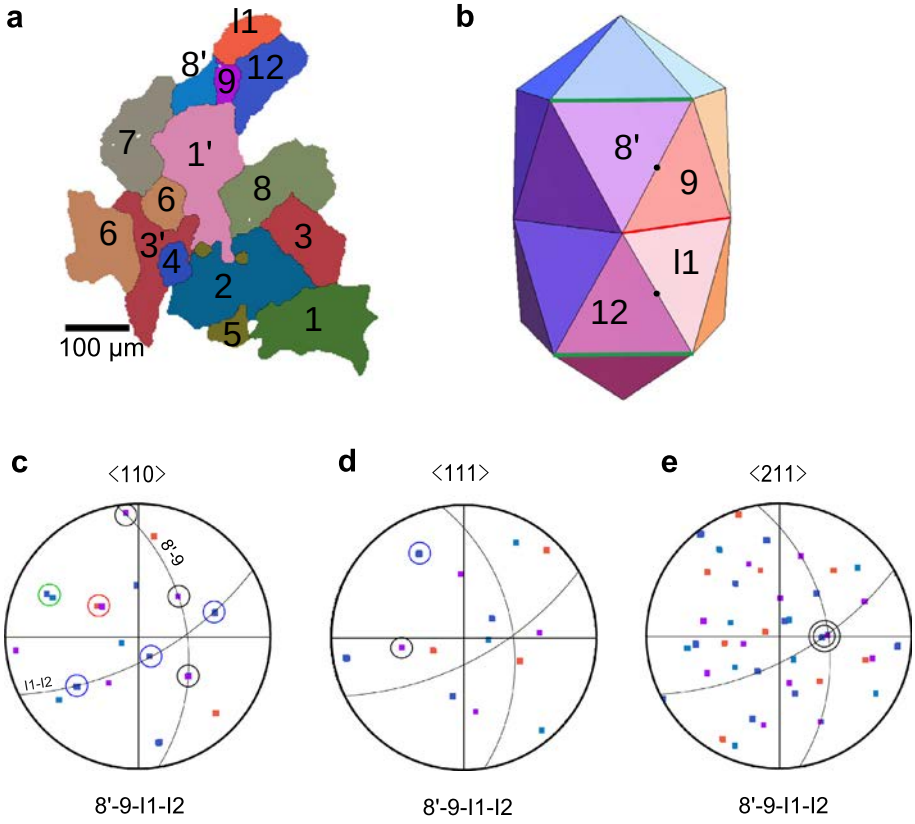

Fig. 7. (a) EBSD reconstructed map of grains in yellow gold alloy with 20 ppm Ir (same as Fig. 6). (b) Schematics of an interlocked icosahedron showing the four facets 8′, 9, I1, I2 on which {1 1 1} planes of the four corresponding Al grains seen in (a) can form to explain their orientation relationship demonstrated by ⟨1 1 0⟩, ⟨1 1 1⟩ and ⟨2 1 1⟩ pole figures (c–e). The common edge between 9 and I1 (in red) and common parallel edge between 8′ and I2 (in green) correspond to common ⟨1 1 0⟩ directions in the pole figure circled with the same color. The common or nearly common {1 1 1} planes are displayed in each pole figure by arcs of circle and common ⟨1 1 0⟩ directions of a twin relationship are shown by a single circle in each pole figure. The ⟨2 1 1⟩ direction common to these four grains is surrounded by a double circle in (e). (For interpretation of the references to color in this figure legend, the reader is referred to the web version of this article.)

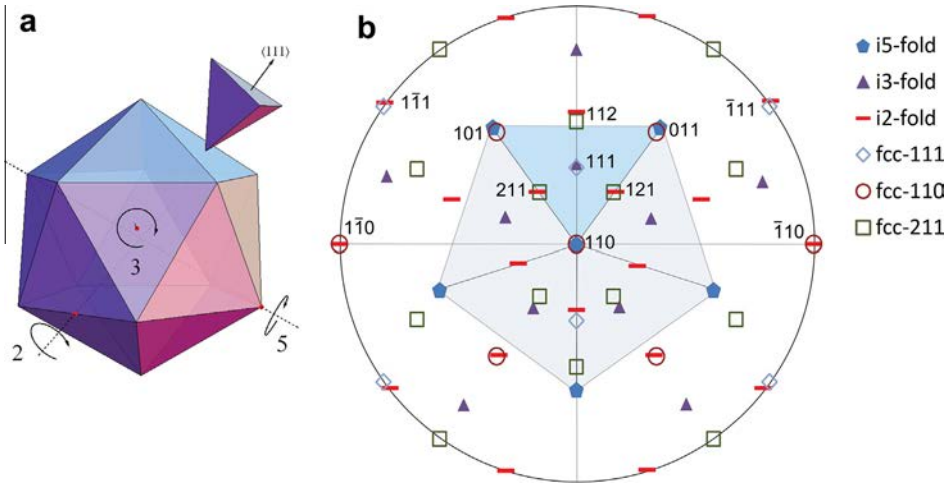

Fig. 8. (a) Representation of the relationship between icosahedral phase and fcc crystal. One fcc crystal is shown by its {1 1 1} planes corresponding to the heteroepitaxial relationship with the icosahedron. (b) Stereographic projection showing orientation relationships between icosahedral phase and an fcc crystal. Pentagons, triangles and rectangles represent 5-fold, 3-fold and 2-fold symmetry axes of the icosahedron seen in (a), respectively. Indices of cubic phase directions close to icosahedral symmetry axes are indicated.

are in a twin relationship; (ii) tetrahedra 9 and I1 share a common ⟨1 1 0⟩ edge (in red); (iii) tetrahedra 8′ and I2 have two parallel ⟨1 1 0⟩ edges (in green); (iv) all four tetrahedra have one parallel ⟨2 1 1⟩ direction (double circled in Fig. 7e), pointing outward of the interlocked icosahedron through the middle of one of their ⟨1 1 0⟩ edges (labeled with a small dot in Fig. 7b).

The six 5-fold symmetry axes of an icosahedron have been revealed by the twin or near-twin orientation relationships of nine fcc neighbor grains. Furthermore, grains 8′, 9, I1 and I2 have an orientation relationship compatible with four adjacent facets of an interlocked icosahedron. All these crystallographic relations constitute very strong evidence for the presence of an icosahedral template on which fcc grains can nucleate and grow with heteroepitaxy relationships: triangular facets/edges of the icosahedron corresponding to the {1 1 1} plane/⟨1 1 0⟩ directions of fcc as shown in Fig. 8a. In Fig. 8b, a stereographic projection has been constructed to show the orientation relationships between the iQC and one of the formed fcc crystals. A 5-fold icosahedral axis and one ⟨1 1 0⟩ axis are placed at the center. Three of the 5-fold iQC symmetry axes nearly correspond to $\langle 1\,1\,0\rangle_{fcc}$ directions, three 2-fold iQC symmetry axes correspond to $\langle 2\,1\,1\rangle_{fcc}$ directions and one 3-fold iQC symmetry axis corresponds to a $\langle 1\,1\,1\rangle_{fcc}$ direction (normal to the iQC facet).

Small misorientations between the icosahedral and cubic axes are due to the small mismatch between a tetrahedron which is deformed to fit into an icosahedron and a regular one. Six 5-fold symmetry axes can be seen on a stereographic projection. Five multiple twinned grains rotated around a common ⟨1 1 0⟩ direction cover the gray colored region of the icosahedron.

It appears that very a small amount of Ir addition into gold alloy promotes the formation of icosahedral solid clusters. The icosahedral phase cannot grow over long distances and generally exists as small clusters with a high surface-to-volume ratio. Icosahedral sites should be preferred to cover large surface and to preserve the icosahedral symmetry, but are energetically unfavorable due to their position [37]. A transition from icosahedral to fcc structures occurs when closed packed sites are occupied by atoms during growth [38]. The heteroepitaxial relationship induces multiple twinning, with gap deficiencies being "concentrated" in a few grain boundaries as growth of the fcc phase proceeds, since coherent twin boundaries exhibit a sharp cusp of minimum interfacial energy. This multitwinned nucleation mechanism shares some similarities with multitwinned nanoparticles of Au and Ag studied in the 1960s [39,40].

4. Conclusion

It has been shown that while Ir addition significantly reduces the grain size in Au–28.4 at.%Cu–16.7 at.%Ag alloys, it also promotes the formation of multiple twinned grains in a way comparable to minute Cr additions to Al–Zn alloys. Several grains are shown to have orientation relationships compatible with the icosahedron or interlocked icosahedron geometry. All our findings point out the existence of a pre-existing quasicrystal phase with 5-fold symmetry, which firstly forms from a supercooled liquid due to its low interfacial energy with the liquid. This mechanism could bring a significant contribution to nucleation phenomena, and could explain the discrepancy between the current rationales and experimental findings. Nevertheless, a small difference exists between Cr:Al–Zn and Ir:Au–Ag–Cu: in the first case, intermediate approximant phases and iQCs are known in Al–Cr system and Cr is peritectic in Al–Zn–Cr, whereas the phase diagram of Ir–Au does not show any intermediate phase. Nevertheless, our observations clearly show that icosahedral order is responsible for nucleation of the fcc phase.

Acknowledgements

The authors thank Rolex SA for its financial support. They also thank the staff of the Interdisciplinary Centre for Electron Microscopy (CIME) of the Ecole Polytechnique Fédérale de Lausanne (EPFL) and in particular Dr. E. Boehm-Courjault for their assistance with the EBSD measurements.

References

[1] Turnbull D. J Appl Phys 1950;21:1022.
[2] Frank FC. Proc R Soc Lond A Math Phys Sci 1952;215:43.
[3] Steinhardt PJ, Nelson DR, Ronchetti M. Phys Rev B 1983;28:784.
[4] Fang XW, Wang CZ, Yao YX, Ding ZJ, Ho KM. Phys Rev B 2011;83:224203.
[5] Reichert H, Klein O, Dosch H, Denk M, Honkimäki V, Lippmann T, et al. Nature 2000;408:839.
[6] Simonet V, Hippert F, Audier M, Bellissent R. Phys Rev B 2001;65:24203.
[7] Schenk T, Holland-Moritz D, Simonet V, Bellissent R, Herlach DM. Phys Rev Lett 2002;89:75507.
[8] Holland-Moritz D, Schenk T, Bellissent R, Simonet V, Funakoshi K, Merino JM, et al. J Non Cryst Solids 2002;312:47.
[9] Shechtman D, Blech I, Gratias D, Cahn JW. Phys Rev Lett 1984;53:1951.
[10] Tsai AP, Guo JQ, Abe E, Takakura H, Sato TJ. Nature 2000;408:537.
[11] Goldman AI, Kong T, Kreyssig A, Jesche A, Ramazanoglu M, Dennis KW, et al. Nat Mater 2013;12:714.
[12] Dubost B, Lang JM, Tanaka M, Sainfort P, Audier M. Nature 1986;324:48.
[13] Tsai A-P, Inoue A, Masumoto T. J Mater Sci Lett 1987;6:1403.
[14] Ohashi W, Spaepen F. Nature 1987;330:555.
[15] Singh A, Tsai AP. J Phys Condens Matter 2008;20:314002.
[16] Zhang H, Wang DH, Kuo KH. Phys Rev B 1988;37:6220.
[17] Zhang H, Wang DH, Kuo KH. J Mater Sci 1989;24:2981.
[18] Srivastava AK, Ranganathan S. Acta Mater 1996;44:2935.
[19] Bolliger B, Dmitrienko VE, Erbudak M, Lüscher R, Nissen H-U, Kortan AR. Phys Rev B 2001;63:52203.
[20] Lüscher R, Erbudak M, Weisskopf Y. Surf Sci 2004;569:163.
[21] Kurtuldu G, Jarry P, Rappaz M. Acta Mater 2013;61:7098.
[22] Cooper MJ. Acta Crystall 1960;13:257.
[23] He ZB, Zou BS, Kuo KH. J Alloys Comp 2006;417:L4.
[24] Ostwald W. Z Phys Chem 1897;22:289.
[25] Herlach D, Galenko P, Holland-Moritz D. Metastable solids from undercooled melts. Oxford: Pergamon Press; 2007.
[26] Lee GW, Gangopadhyay AK, Croat TK, Rathz TJ, Hyers RW, Rogers JR, et al. Phys Rev B 2005;72:174107.
[27] Kelton KF, Lee GW, Gangopadhyay AK, Hyers RW, Rathz TJ, Rogers JR, et al. Phys Rev Lett 2003;90:195504.
[28] Henry S, Rappaz M, Jarry P. Metall Mater Trans A 1998;29:2807.
[29] Salgado-Ordorica MA, Rappaz M. Acta Mater 2008;56:5708.
[30] Nielsen JP, Tuccillo JJ. J Dent Res 1966;45:964.
[31] Ott D, Raub CJ. Gold Bull 1981;14:69.
[32] Renner H, Schlamp G, Hollmann D, Lüschow HM, Tews P, Rothaut J, et al. Ullmann's Encycl Ind Chem 2000.
[33] Mackenzie JK. Biometrika 1958;45:229.
[34] Warrington DH, Boon M. Acta Metall 1975;23:599.
[35] Reed RP, Schramm RE. J Appl Phys 1974;45:4705.
[36] Hasson GC, Goux C. Scr Metall 1971;5:889.
[37] Martin TP. Phys Rep 1996;273:199.
[38] Farges J, De Feraudy MF, Raoult B, Torchet G. J Chem Phys 1986;84:3491.
[39] Ino S. J Phys Soc Japan 1966;21:346.
[40] Ino S. J Phys Soc Japan 1969;27:941.